
Neuroevolution-Enhanced Multi-Objective Optimization for Mixed-Precision Quantization

Santiago Miret ^{*†} **Vui Seng Chua** [†] **Mattias Marder** **Mariano Phielipp** **Nilesh Jain**
Intel Labs Intel Labs Intel Israel Intel Labs Intel Labs

Somdeb Majumdar
Intel Labs

Abstract

Mixed-precision quantization is a powerful tool to enable memory and compute savings of neural network workloads by deploying different sets of bit-width precisions on separate compute operations. Recent research has shown significant progress in applying mixed-precision quantization techniques to reduce the memory footprint of various workloads, while also preserving task performance. Prior work, however, has often ignored additional objectives, such as bit-operations, that are important for deployment of workloads on hardware. Here we present a flexible and scalable framework for automated mixed-precision quantization that optimizes multiple objectives. Our framework relies on Neuroevolution-Enhanced Multi-Objective Optimization (NEMO), a novel search method, to find Pareto optimal mixed-precision configurations for memory and bit-operations objectives. Within NEMO, a population is divided into structurally distinct sub-populations (species) which jointly form the Pareto frontier of solutions for the multi-objective problem. At each generation, species are re-sized in proportion to the goodness of their contribution to the Pareto frontier. This allows NEMO to leverage established search techniques and neuroevolution methods to continually improve the goodness of the Pareto frontier. In our experiments we apply a graph-based representation to describe the underlying workload, enabling us to deploy graph neural networks trained by NEMO to find Pareto optimal configurations for various workloads trained on ImageNet. Compared to the state-of-the-art, we achieve competitive results on memory compression and superior results for compute compression for MobileNet-V2, ResNet50 and ResNeXt-101-32x8d, one of the largest ImageNet models amounting to a search space of $\sim 10^{146}$. A deeper analysis of the results obtained by NEMO also shows that both the graph representation and the species-based approach are critical in finding effective configurations for all workloads.

1 Introduction

Recent advances in deep learning have partially been driven by rapid growth in the size and complexity of deep neural network (DNN) architectures [Dean et al., 2012, Ying et al., 2018]. This growth in complexity, along with a desire to deploy deep neural network workloads on various types of hardware, has spurred a significant need for advances in memory and compute compression techniques for DNN workloads. We define memory compression as reduction in workload memory footprint, and compute compression as the reduction of bit-operations during workload inference, which correlates to both latency and power consumption improvements during hardware deployment. The total bit-operations

*Correspondence to: <santiago.miret@intel.com>

[†]Equal Contribution

of a workload is defined as the number of Multiply-Add-Accumulation (MAC) operations multiplied by the compute precision. Studies have shown that high-throughput low-precision compute devices consume lower power compared to floating-point units while also achieving lower latency [Nvd, Int, Rodriguez et al., 2018].

In this work we focus on mixed-precision quantization [Habi et al., 2020, Uhlich et al., 2019, Wang et al., 2019, Dong et al., 2019], a subset of quantization methods that reduce model weights and activations to a heterogeneous set of bit-widths throughout the model. The goal of bit-width reduction is to decrease a model’s memory footprint and reduce latency at inference time with minimal degradation of task performance. Common approaches to mixed-precision quantization focus on optimizing one particular feature, usually the model memory footprint [Dong et al., 2019, Uhlich et al., 2019]. Conversely, our approach, which is outlined in Figure 1, frames mixed-precision quantization as a multi-objective problem where we aim to find the Pareto optimal set of mixed-precision configurations that express the optimal trade-offs between various metrics of interests. In this work we focus our multi-objective optimization approach on three distinct objectives for each workload: task performance, model size (memory), and compute complexity (bit-operations).

We determine our multi-objective solutions through our novel method Neuroevolution-Enhanced Multi-Objective Optimization (NEMO), which combines classical multi-objective search algorithms [Konak et al., 2006] with neuroevolution methods that search directly on the parameters of a neural network [Such et al., 2017, Khadka et al., 2019]. NEMO manages structurally distinct sub-populations, referred to as species, including neural network and non-neural network representations, via a dynamic allocation technique leveraging a multi-bandit approach and multi-objective utility functions.

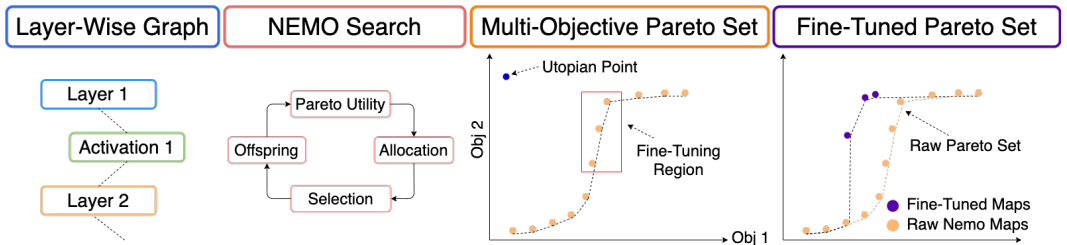


Figure 1: Major Steps: First we refactor a workload into a layer-wise graph; second we apply NEMO to search for a Pareto optimal set in multiple dimensions; third we select a region of interest for fine tuning select configurations; fourth we report the final Pareto optimal set containing fine-tuned maps

Based on our approach, we make the following contributions, which to best of our knowledge are novel contributions to the field of neural network quantization and compression:

1. **Multi-Objective Formulation for Mixed-Precision Quantization:** We create a multi-objective framework for mixed-precision quantization leading to a Pareto optimal set of solutions expressing the trade-offs related to various metrics relevant for model compression. We evaluate our method on various ImageNet [Deng et al., 2009] workloads, including ResNeXt-101-32x8d [Xie et al., 2017] one of the largest ImageNet models.
2. **Graph Representation:** We develop a graph-based representation of the neural network workloads allowing us to leverage graph neural networks to find suitable mixed-precision configurations for the weights and activations of the compressed workloads.
3. **NEMO:** a gradient-free, scalable, multi-objective training method enabling both traditional search methods and neuroevolution techniques through distinct species in its population. NEMO improves on established search methods, such as NSGA-III [Deb and Jain, 2013], by dynamically managing structurally distinct species in its population based on the quality of their contribution to overall Pareto frontier. In this work, NEMO successfully trains GNN representations to find Pareto optimal mixed-precision configurations using neuroevolution.

2 Related Work

Quantization: Deep neural network compression via quantization has become increasingly prevalent in recent years, as evident by INT8 quantization support by major deep learning frameworks [Paszke

et al., 2019, Abadi et al., 2015] and hardware vendors [int, nvi] enabling developers to perform efficient model quantization. The research community has continued to push the state of the art in quantization methods through various approaches, including quantization-aware training [Jain et al., 2019, Esser et al., 2020], data-free quantization methods [Nagel et al., 2019, Haroush et al., 2020], as well as post-training [Li et al., 2021] and mixed-precision quantization. Recent mixed-precision quantization research, such as DQ [Uhlich et al., 2019], DNAS [Wu et al., 2018] and HAQ [Wang et al., 2019], has generally focused on solving a constrained optimization problem where memory compression is optimized while maintaining a minimal, acceptable accuracy drop. Further advances, such as HAWQ-V3 from Yao et al. [2020] and HMQ from Habi et al. [2020] developed mixed-precision quantization techniques considering hardware-aware metrics for further optimization. Yao et al. [2020] created a hardware-aware mixed-precision quantization method leveraging integer linear programming and measured bit-operations as a surrogate metric for hardware performance. Habi et al. [2020] developed a mixed-precision quantization block, which is applied to the workload to find uniform and symmetric bit-widths for the given block. Habi et al. [2020] also reported Pareto frontiers for Cifar-10 [Krizhevsky et al.] and ImageNet [Deng et al., 2009] workloads in two dimensions, accuracy and memory compression. Our work, by contrast, reports a Pareto frontier in three relevant dimensions including accuracy, memory compression and bit-operations as a surrogate metric for hardware performance, and can be easily extended to more objectives depending on the broader task or specific user needs. We also develop a graph representation of the workload inspired by Khadka et al. [2020] allowing us to leverage graph convolutions trained by gradient-free neuroevolution, which to the best of our knowledge is a novel approach to mixed-precision quantization.

Multi-Objective Search: Our mixed-precision quantization technique is enabled by NEMO, which differentiates from traditional multi-objective evolutionary search algorithms [Konak et al., 2006] and past neuroevolution techniques, such as MM-NEAT [Schrum and Miikkulainen, 2016, Miikkulainen, 2015, van Willigen et al., 2013], and more recent algorithmic variations [Künzel and Meyer-Nieberg, 2020, Steven, 2018] in a couple of meaningful ways: NEMO enables dynamic species management between structurally distinctive species, including GNN based species and model free species that search directly in the solution space. This enables architectural diversity across the population, including distinct mutation and crossover operations for each species, to operate together in a unified framework. Prior work [Stanley and Miikkulainen, 2002, Abramovich and Moshaiov, 2016], conversely, usually applied similar mutation and crossover operations across species to achieve diversity in the solution space. Moreover, as described in more detail in Section 3.2, NEMO leverages multi-objective utility metrics measured for each species with multi-bandit methods in an integrated framework that can be applied to large variety of search problems beyond the mixed-precision quantization setting described in this work.

3 Method

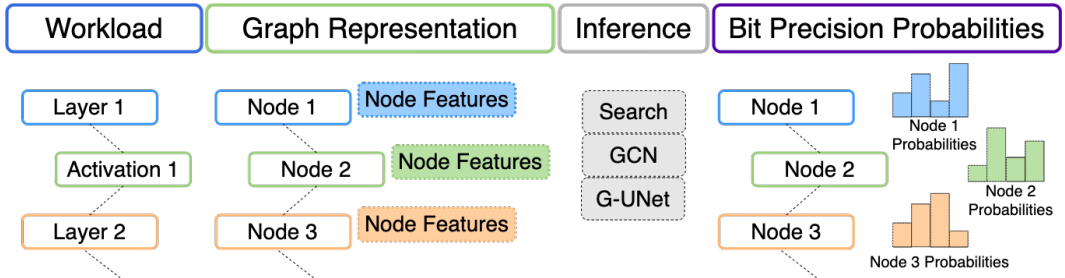


Figure 2: Bit-Precision Selection For A Workload: 1. We transform the workload into a sequential graph; 2. We perform an inference method of choice on the graph (direct search on the bit-widths or Graph Neural Network inference); 3. We select the bit-width based on the resulting probabilities

Our method is based on the integration of three techniques: 1. Formulating layer-wise mixed-precision quantization of a workload as a multi-objective search problem as described in Section 3.1. 2. Refactoring of the workload into a sequential graph representation suitable for GNNs. 3. Finding a Pareto optimal set of solutions using NEMO as described in Section 3.2 followed by fine tuning of a subset precision maps as described in Section 3.3. We create our graph representation by declaring

each quantizable operation in the workload as a node and build the edges by connecting the nodes sequentially, meaning $\mathcal{G}_{\text{edges}} = \{n_1 \rightarrow n_2, n_2 \rightarrow n_3, \dots\}$, where n corresponds to the graph nodes representing computational operations in the targeted workload. The node features of the graph representation consist of a concatenation of a one-hot encoding of the given operation and eight general features associated with the operation described in detail in Appendix C.1. After constructing the workload graph, we perform inference on the nodes of the graph either by direct search or with a graph neural network as shown in Figure 2. Each inference method, including different GNN architectures, is codified as a distinct species within NEMO as described in Section 3.2.

3.1 Mixed-Precision Quantization

We perform uniform affine quantization, the predominant approach for quantized neural network inference [Krishnamoorthi, 2018, Gholami et al., 2021]. Affine quantization maps neural network weight and activation tensors of 32-bit floating point precision to a finite set of fixed points defined by the quantization bit width. Specifically, we employ asymmetric affine quantization, enabling separate bit-width selection for both weights and activations, with multiple quantizers q defined as:

$$q(\mathbf{x}; \mathbf{b}) = \left\lfloor \frac{\text{clamp}(x; x_{\min}, x_{\max})}{s} + z \right\rfloor; \quad s = \frac{x_{\max} - x_{\min}}{2^b - 1}; \quad z = \frac{-x_{\min}}{s} \quad (1)$$

Each quantizer q maps the elements $x \in \mathbb{R}$ of a tensor \mathbf{x} to a quantized value corresponding to one of the integers $\{-2^{b-1}, -2^{b-1} + 1, -2^{b-1} + 2, \dots, 2^{b-1} - 1\}$, and is parameterized by the bit width b , as well as x_{\min}, x_{\max} corresponding to the thresholds of the dynamic range of the tensor \mathbf{x} which are calibrated based on the elements of tensor. As shown in Equation (1), $\{b, x_{\min}, x_{\max}\}$ collectively define the scale factor s and zero point z . s denotes the step size in x representing a unit delta between two adjacent integers, and z corresponds to the value in x which maps to the zero quantized value. Effectively, each quantizer q first saturates the tensor \mathbf{x} by $\text{clamp}(x; x_{\min}, x_{\max}) := \min(\max(x; x_{\min}), x_{\max})$, then scales the saturated tensor by s , adds the offset z and finally rounds the resulting tensor elements to the nearest integer. Effective quantization can reduce the memory footprint of a workload and also increase inference speed by enabling efficient usage of high throughput low-precision computational units. These benefits of quantization, however, usually come at the cost of lower performance of the neural network on its desired task. Given these inherent trade-offs between task performance, memory footprint and computational throughput, we formulate finding fine-grained quantizer bit-widths as a multi-objective search problem. Given an L -layer trained neural network N , we search for the set of bit widths \mathcal{B} consisting of weights (b_w^l) and activations (b_a^l) for each layer subject to K objectives:

$$\mathcal{B} = \{b_w^0, b_a^0, b_w^1, b_a^1, \dots, b_w^L, b_a^L\} \quad \forall l \in L \quad \text{s.t.} \quad \{obj_0(N^l), obj_1(N^l), \dots, obj_k(N^l)\} \quad \forall k \in K$$

As shown in greater detail in Figure 2 and Figure 3, we obtain a Pareto optimal of mixed-precision configuration \mathcal{B} by leveraging a combination of direct search and graph neural network inferences, both of which are trained and refined by our NEMO method.

3.2 Neuroevolution-Enhanced Multi-Objective Optimization

Neuroevolution-Enhanced Multi-Objective Optimization (NEMO), shown in Figure 3 and outlined Algorithm 1, is a multi-objective evolutionary search algorithm with the capability of managing multiple species. Many of the components of the NEMO algorithm can be tailored towards different needs and preferences, e.g. species types may contain various architectures and utility metrics can express any underlying property one aims to optimize. As described in Algorithm 1, NEMO manages both species level and individual level variables. Species level variables include the utility metric $u_{s \in \mathcal{S}}$, the species allocation $a_{s \in \mathcal{S}}$, as well as the mutation $\mathcal{M}_{s \in \mathcal{S}}$ and crossover operations $\mathcal{C}_{s \in \mathcal{S}}$. Individual level variables, which are tracked for each individual in the population regardless of the species include the fitness $\mathcal{F}_{p \in \mathcal{P}}$ and the rank $r_{p \in \mathcal{P}}$.

In this study, we deploy three distinct species: a classical search species that searches directly on the bit-widths and two GNN based species (variations of GCN-Conv [Kipf and Welling, 2016] and Graph U-Net [Gao and Ji, 2019]). For the direct search species we apply bounded simulated binary crossover and polynomially bounded mutation. The parameter values for each node range from $[0, 1]$, which are then converted to four mixed-precision bit-widths of $\{1, 2, 4, 8\}$ corresponding to $[0, 0.25)$, $[0.25, 0.5)$, $[0.5, 0.75)$, $[0.75, 1]$ respectively. For the GNN based species we adopt sub-structure neuroevolution where the operations are applied on the weights on individual layers in the

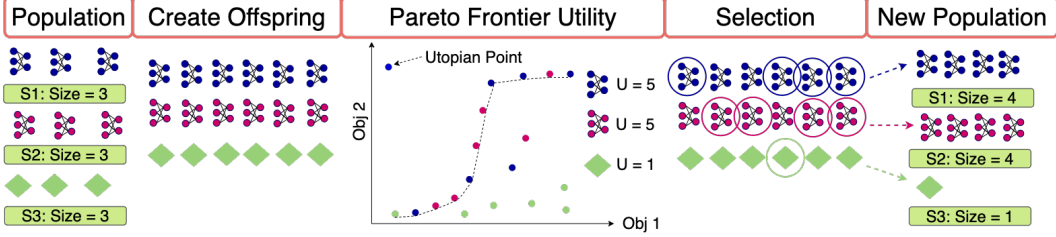


Figure 3: An example NEMO generation for a population \mathcal{P} with $\mathcal{P}_{size} = 9$ containing three species $s \in \mathcal{S}$ of equal size $s_{size} = 3$: {Neuroevolution Species #1 (S1 - blue networks), Neuroevolution Species #2 (S2 - magenta networks) and Search Species (S3 - green diamond)}. At the beginning of a generation each species produces offspring, doubling the number of members in each species. NEMO then computes the utility metrics for each species (in the illustration above the utility is the number of solutions in the Pareto frontier) as well as each species’ respective size allocations. Finally, the best-performing members within each species’ size allocations are selected for the next generation.

Algorithm 1 Generalized NEMO Algorithm

- 1: Initialize a population \mathcal{P} with individuals p contained in a set of species $p \in s \in \mathcal{S} \subset \mathcal{P}$
 - 2: Define species specific mutation operation $\mathcal{M}_{s \in \mathcal{S}}$ and crossover operation $\mathcal{C}_{s \in \mathcal{S}}$
 - 3: Initialize an allocation method $\mathcal{A}_{\mathcal{P}}$, a utility function $\mathcal{U}_{\mathcal{P}}$ describing the utility of each species $s \in \mathcal{S}$ and a ranking method $\mathcal{R}_{\mathcal{P}}$ for the population \mathcal{P}
 - 4: Define stopping criteria (e.g. maximum number of generations)
 - 5: Evaluate the fitness $\mathcal{F}_{p \in \mathcal{P}}$ for each member of the population (e.g [accuracy, memory, bit-ops])
 - 6: **while** training NEMO **do**
 - 7: **for** each generation **do**
 - 8: Apply mutations $\mathcal{M}_{s \in \mathcal{S}}$ and crossovers $\mathcal{C}_{s \in \mathcal{S}}$ to create offspring $\mathcal{O}_{s \in \mathcal{S}}$
 - 9: Evaluate the fitness $\mathcal{F}_{p \in \mathcal{O}}$ for each member in the offspring
 - 10: Compute the utility $u_{s \in \mathcal{S}}$ for each species using \mathcal{U}
 - 11: Compute the allocation $a_{s \in \mathcal{S}}$ for each species using \mathcal{A}
 - 12: Compute the rank $r_{p \in \mathcal{P}}$ for each member of population using \mathcal{R}
 - 13: **for** $s \in \mathcal{S}$ **do**
 - 14: Fill $a_{s \in \mathcal{S}}$ starting with the highest ranked members of the species $p \in s \subset \mathcal{P}$
-

neural network. In this case, the crossover operation is an average of two randomly chosen layers in two neural networks and the mutation operation is the addition of Gaussian noise to the weights of a randomly selected layer. The bit-width values are chosen according to the logits output of GNN, which represent probabilities for each bit-width as shown in Figure 2. We define the R2-Indicator [Hansen and Jaszkiwicz, 1994], with a set of uniform weight vectors Λ , as the utility metric for each species $u_{s \in \mathcal{S}}$. The R2 corresponds to the averaged sum of the minimum distances for all solutions $a \in A$, where a is analogous to $\mathcal{F}_{p \in \mathcal{P}}$ above, in any dimension over each weight vector $\lambda \in \Lambda$:

$$R2(A) = R2(A, \Lambda, z^*) = \frac{1}{|\Lambda|} \sum_{\lambda \in \Lambda} \min_{a \in A} \left\{ \max_{i \in \{1, \dots, k\}} \{\lambda_i | z_i^* - a_i| \} \right\} \quad (2)$$

z^* above corresponds to an utopian point that represents the best possible solution (in the case of mixed-precision quantization the utopian point represents 100% accuracy, 0 bytes model-size and 0 bit-ops). As discussed in Steven [2018], Künzel and Meyer-Nieberg [2020], minimizing the R2 indicator for a given set of solutions incentivizes the algorithm to find solution closer to the utopian point z^* , which is a good fit our purposes. Another potentially promising choice of utility metric is the hypervolume spanned by a given Pareto front [Steven, 2018, Künzel and Meyer-Nieberg, 2020]. Our setup with multiple species, however, can easily lead to overlapping hypervolumes making it more challenging to attribute the set-wise contribution of a species compared to the R2-Indicator. To determine species size allocation we compute an upper confidence bound (UCB) score $\mathcal{A}_{s \in \mathcal{S}}$ [Auer, 2002] commonly used in multi-bandit problems [Bubeck et al., 2012, Karnin et al., 2013] given by:

$$\mathcal{A}_{s \in \mathcal{S}} = v_s + c * \sqrt{\frac{\log(\sum_{s \in \mathcal{S}} y_s)}{y_s}} \quad (3)$$

where v_s is the utility (R2 value) and y_s is the number of evaluations of the species respectively. For ranking and selection we apply a variant of NSGA-III by Deb and Jain [2013], where we rank the individuals in the entire population based on their multi-objective solution vectors and then fill the size allocation of each species based on the overall NSGA-III population ranking. If any species has leftover allocation after the filling process, we create an additional set of random offspring to fill its remainder and continue to the next generation.

3.3 Fine Tuning Procedure

The Pareto optimal set of mixed-precision configurations determined by NEMO often heavily degrade the accuracy of the underlying workload due to aggressive quantization. To mitigate this degradation of accuracy, we perform quantization-aware training (QAT) [Kozlov et al., 2020] on a subset of maps in the Pareto frontier to improve their accuracy. We maintain the same bit widths, but fine-tune network parameters, along with the dynamic range threshold $w_{min}^l, w_{max}^l, a_{min}^l, a_{max}^l$ using straight-through gradient estimation [Bengio et al., 2013] for the non-differentiable quantization operators during backpropagation. Formally, the fine-tuning procedure optimizes the task loss of L -layer quantized neural network N' with M data points by:

$$\min \mathcal{L}(x_i, y_i; w_{min}^l, w_{max}^l, a_{min}^l, a_{max}^l, \mathbf{w}^l), \forall l \in L, \forall i \in M \quad (4)$$

4 Experiments & Results

We perform our experiments on different ImageNet workloads (MobileNet-V2 [Sandler et al., 2018], ResNet50 [He et al., 2016], ResNeXt-101-32x8d [Xie et al., 2017]) based on pre-trained models provided in TorchVision [Paszke et al., 2019], and leverage NNCF by Kozlov et al. [2020] to build simulated quantization layers for the weights and activations in the workload. While NNCF supports many quantization modes and settings, our experiments leverage asymmetric affine quantization to provide maximum flexibility for finding optimal configurations. NNCF initializes the dynamic threshold of each quantizer by calculating the statistical mean across a number of batches from the inference data. Following calibration, we take the data from the NNCF representation of the quantized network and convert it to graph form as described in Section 3. We allow our search algorithm to choose from a set of four different bit-widths: $\{1, 2, 4, 8\}$ and perform a multi-objective optimization using NEMO to obtain a set of Pareto optimal precision maps based on the following objectives:

- **Task Performance:** $\max(\text{Top5 Accuracy})$ of the given workload on a stratified subset of the ImageNet training data consisting of 5 images per class leading to a total of 5000 images. The stratified sample enables us to perform faster evaluations during the search process. We optimize Top5 accuracy to achieve less noisy evaluations during search and report results in Top1 accuracy for easier comparison with prior work.
- **Memory Compression:** $\min(\text{Model-Ratio})$ of a given workload that expresses the ratio of the reduced memory footprint of model parameters compared to the full-precision footprint.
- **Compute Compression:** $\min(\text{Bit-Operation Ratio})$ of a given workload that outlines the ratio of reduced complexity compared to full-precision complexity.

NEMO then finds a three-dimensional Pareto frontier of optimal precision maps based on our stratified sampling of the ImageNet data. Subsequently, we re-evaluate the Pareto set of configurations on the full ImageNet data and select a subset of precision maps for fine-tuning to improve the accuracy of the corresponding mixed-precision configurations for the given workload. We determine the fine-tuning subset based on their proximity to a region of interest, described by the model-ratio and bit-ops ratio, that is heuristically known to include significant changes in accuracy for quantized workloads.

4.1 Multi-Objective Pareto Optimal Sets

The combinatorial complexity of each experiments increases exponentially with the number quantizable operations for each workload. MobileNet-V2 contains 116 quantizable operations, leading to a combinatorial complexity of 4^{116} or $\sim 10^{69}$; ResNet50 includes 124 quantizable operations ($\sim 10^{74}$), and ResNeXt-101-32x8d contains 244 quantizable operations with a complexity of $\sim 10^{146}$.

ResNeXt-101-32x8d: The three-objective Pareto front found by NEMO illustrated in Figure 4 contains 264 unique solutions. Given its large size, fine-tuning experiments for this workload

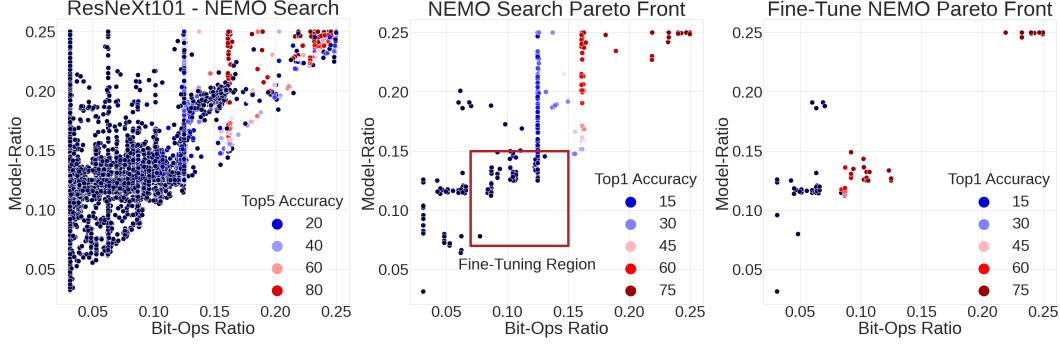


Figure 4: Heatmaps of ResNeXt-101-32x8d Solutions: All NEMO search results (left), preliminary Pareto set with highlighted fine-tuning region (middle), and final Pareto set after fine-tuning.

are significantly more expensive compared to other workloads, leading us to select a small fine tuning region spanning $0.07 \leq \text{model - ratio} \leq 0.15$, $0.07 \leq \text{bit - ops} \leq 0.15$ shown by the red rectangular region. The final fine-tuned NEMO Pareto frontier contains 54 unique configurations as fine-tuned solutions make others sub-optimal. We did not find previous literature on mixed-precision quantization of ResNeXt-101-32x8d to compare our results against and report two-dimensional projections of the full Pareto frontier in Figure 5, which show the significant improvements in Top1 accuracy made by the fine-tuning procedure for the NEMO Pareto frontier.

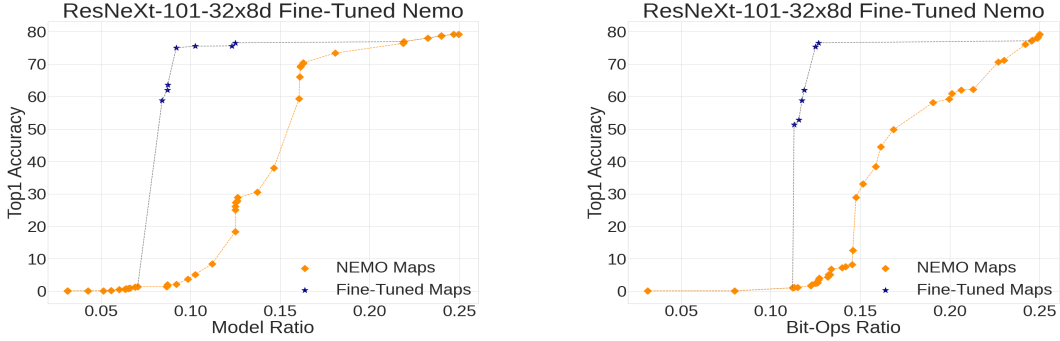


Figure 5: ResNeXt-101-32x8d: Two-Dimensional Projections of Pareto Fronts for Top1-Accuracy vs Model-Ratio (left) and Top1-Accuracy vs Bit-Ops for fine-tuned configurations (right)

MobileNet-V2: The initial search yields a Pareto front of 384 unique solutions from which we then downselect a region spanning $0.07 \leq \text{model - ratio} \leq 0.20$, $0.05 \leq \text{bit - ops} \leq 0.20$ for further fine-tuning. Our final, fine-tuned NEMO Pareto front, shown in Figure D.1 in the appendix, contains 112 unique solutions. We show how our solutions in corresponding neighborhoods of memory compression compare to HAQ [Wang et al., 2019] and HMQ [Habi et al., 2020] based on reported Top1 Accuracy, compression ratio, and bit-ops in Table 1. Since bit-ops were not reported in either paper, we infer the bit-ops based on the information about the final quantized workload as described in the respective papers when possible. We observe that the configurations in the fine-tuned NEMO Pareto frontier are generally competitive in memory compression and state-of-the-art in compute compression. Full 2D projection Pareto fronts are shown in the appendix in Figure D.2.

ResNet50: Our initial NEMO search yields 266 Pareto optimal configurations from which we select a fine-tuning region spanning $0.08 \leq \text{model - ratio} \leq 0.20$, $0.08 \leq \text{bit - ops} \leq 0.13$. The final fine-tuned NEMO Pareto set, shown in Figure D.3 in the appendix, includes 73 unique optimal configurations. We compare to HAQ, HMQ in similar memory compression neighborhoods in Top1 Accuracy, compression ratio, and bit-ops in Table 2. Similar to MobileNet-V2, we infer bit-ops based on reported results when possible. We observe that the configurations in the fine-tuned NEMO Pareto set are mostly weaker Top1 accuracy than previous work in memory compression, but show significant improvement in compute compression. Most previous work aimed to optimize memory compression with limited impact to Top1 accuracy and hence prescribed uniform bit widths for

Method	Top1 (%)	Size Ratio	Memory Compression	Bit-Ops Ratio	Compute Compression	w-space	a-space	Avg. w-bits	Avg. a-bits
Baseline	71.88	1	1×	1	1×	FP32	FP32	32	32
HAQ	66.70	0.071	14.1×	1.000	1.0×	{1...8}	FP32	NR	32
HMQ	65.70	0.069	14.4 ×	0.250	4.0×	{2...8}	8-bit	NR	8
NEMO	68.39	0.071	14.1×	0.194	5.2 ×	{1,2,4,8}	{1,2,4,8}	5.63	4.13
HAQ	70.90	0.103	9.7×	1.000	1.0×	{1...8}	FP32	NR	32
HMQ	70.12	0.103	9.7×	0.250	4.0×	{2...8}	8-bit	NR	8
NEMO	68.66	0.091	11.0 ×	0.195	5.1 ×	{1,2,4,8}	{1,2,4,8}	5.58	4.77
HAQ	71.47	0.134	7.5×	1.000	1.0×	{1...8}	FP32	NR	32
HMQ	70.91	0.130	7.7×	0.250	4.0×	{2...8}	8-bit	NR	8
NEMO	70.82	0.126	8.0 ×	0.199	5.0 ×	{1,2,4,8}	{1,2,4,8}	6.19	4.83
NEMO	70.24	0.122	8.2×	0.181	5.5 ×	{1,2,4,8}	{1,2,4,8}	4.77	4.96

Table 1: MobileNet-V2 neighborhoods of similar solutions in high, mid-range and low memory compression ranges. NEMO achieves better compute compression for all neighborhoods. The last row shows a solution with superior compute compression for minimal accuracy loss.

activation tensors, which are independent from the model size. While high activation precisions are advantageous for task performance, they preclude efficient usage of mixed-precision compute acceleration, demonstrating a clear trade-off between the objectives. Our method, conversely, is fairly unconstrained compared to previous approaches, as we determine bit-widths for all weights and activations tensors, while also optimizing for an additional compute compression objective that encompasses further trade-offs. We believe the significant improvements in compute compression compared to prior work show the promise of our approach, and also think that search space reduction methods can be complimentary to our method. Narrowing the search space via Hessian sensitivities, while also optimizing for compute compression, for example, could be a promising future direction which Yao et al. [2020] already started to explore.

Method	Top1 (%)	Size Ratio	Memory Compression	Bit-Ops Ratio	Compute Compression	w-space	a-space	Avg. w-bits	Avg. a-bits
Baseline	76.15	1	1×	1	1×	FP32	FP32	32	32
HAQ	70.63	0.065	15.5×	1.000	1.0×	{1...8}	FP32	NR	32
HMQ	75.00	0.064	15.7 ×	0.250	4.0×	{2...8}	8-bit	NR	8
NEMO	70.71	0.085	11.8×	0.194	5.2 ×	{1,2,4,8}	{1,2,4,8}	5.58	3.17
HAQ	75.30	0.095	10.6×	1.000	1.0×	{1...8}	FP32	NR	32
HMQ	76.10	0.092	10.9 ×	0.250	4.0×	{2...8}	8-bit	NR	8
NEMO	72.91	0.093	10.7×	0.141	7.1 ×	{1,2,4,8}	{1,2,4,8}	4.34	3.44
HAQ	76.14	0.125	8.0×	1.000	1.0×	{1...8}	FP32	NR	32
HMQ	76.30	0.111	9.0×	0.250	4.0×	{2...8}	8-bit	NR	8
NEMO	75.84	0.108	9.3 ×	0.164	6.1 ×	{1,2,4,8}	{1,2,4,8}	5.86	4.11
NEMO	75.51	0.125	8.0×	0.127	7.9 ×	{1,2,4,8}	{1,2,4,8}	4.00	4.68

Table 2: ResNet50 neighborhoods of similar solutions in high, mid-range and low memory compression ranges. NEMO achieves better compute compression for all neighborhoods. The last row shows a solution with superior compute compression for minimal accuracy loss.

4.2 NEMO Search Analysis

One of the major innovations of NEMO is the dynamic allocation of different pre-defined species in the search framework. As such, we wanted to assess the effects of having different species in the search method: We present the percentage of Pareto frontier members for each of the species in Figure 6 and the percent of total evaluations per species throughout the search process in Figure 7.

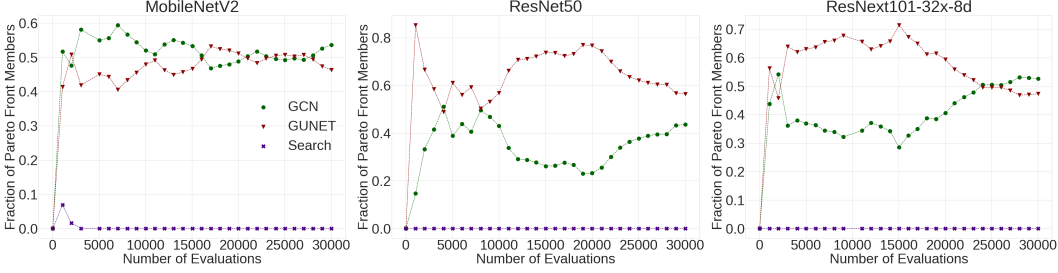


Figure 6: Percentage of Members in the Pareto Optimal Frontier for Different Species in NEMO

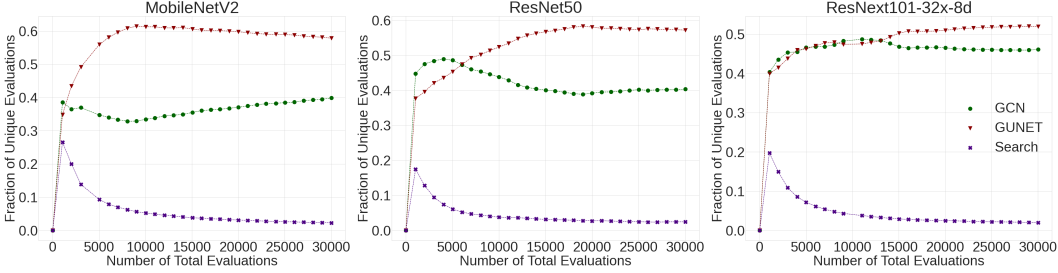


Figure 7: Percentage of Unique Evaluations for Different Species in NEMO

The data in Figure 6 show that both GNN species contribute significantly to the Pareto frontier, with Graph-UNet generally contributing more for the larger workloads, ResNet50 and ResNeXt-101-32x8d. This showcases the importance of the GNN species and the graph embedding described in Section 3, especially since the direct search contributes very insignificantly to the Pareto frontier throughout the search. In Figure 7 we see the percentage of unique evaluations performed by each species throughout the search, which again highlight the importance of the GNN based species. Figure 7 also shows how NEMO chooses to allocate different species’ size given that a larger percentage of evaluations per epoch indicates a larger allocation for the respective species in that generation. The data show that NEMO generally allocates the majority of its size budget to the Graph-UNet species across all three workloads, which appears to be a good choice given the high representation of Graph-UNet solutions in the Pareto frontier. We also observe that NEMO gradually decreases the allocation of the direct stateless search, which fails to provide additions to the Pareto frontier. Lower direct search allocations then allow NEMO to devote more resources to finding better solutions via the GNNs.

5 Discussion

Limitations & Future Work: One limitation of our method is that it does not achieve state-of-the-art results along all objectives for all tested workloads, particularly ResNet50. As discussed in Section 4.1, a plausible reason for that shortcoming is our relatively unconstrained search space is probably too large for NEMO to search effectively. Other methods, such as HAWQ-V2 [Dong et al., 2019], reduce the search space with effective priors, and we think that promising future work could leverage those insights to determine better mixed-precision configurations. Our method also heavily relies on an effective graph representation and pre-determined GNN architectures that act as species within NEMO. Future work could address this by discovering new species automatically, similar to an AutoML method and NEAT’s historical markings [Stanley and Miikkulainen, 2002]. Moreover, we only show results on ImageNet models, which are significantly smaller than language models, such as BERT [Devlin et al., 2018], whose greater parameter space would make the search even more challenging. Beyond this study, we also see promise in applying our method to other compression settings, such as sparsification and filter pruning, as well as to multi-objective problems in different domains. Finally, all results on mixed-precision quantization, including our own, are reported on simulation and not an actual hardware runs. Future experiments on real hardware could show how mixed-precision quantized models perform for the various objectives we discussed.

References

- Intel® deep learning boost - intel® ai. URL <https://www.intel.com/content/www/us/en/artificial-intelligence/deep-learning-boost.html>.
- Nvidia tensor cores: Versatility for hpc & ai. URL <https://www.nvidia.com/en-us/data-center/tensor-cores/>.
- Intel OpenVINO Toolkit. URL <https://software.intel.com/content/www/us/en/develop/tools/openvino-toolkit.html>.
- Nvidia TensorRT. URL <https://developer.nvidia.com/tensorrt>.
- Martín Abadi, Ashish Agarwal, Paul Barham, Eugene Brevdo, Zhifeng Chen, Craig Citro, Greg S. Corrado, Andy Davis, Jeffrey Dean, Matthieu Devin, Sanjay Ghemawat, Ian Goodfellow, Andrew Harp, Geoffrey Irving, Michael Isard, Yangqing Jia, Rafal Jozefowicz, Lukasz Kaiser, Manjunath Kudlur, Josh Levenberg, Dan Mané, Rajat Monga, Sherry Moore, Derek Murray, Chris Olah, Mike Schuster, Jonathon Shlens, Benoit Steiner, Ilya Sutskever, Kunal Talwar, Paul Tucker, Vincent Vanhoucke, Vijay Vasudevan, Fernanda Viégas, Oriol Vinyals, Pete Warden, Martin Wattenberg, Martin Wicke, Yuan Yu, and Xiaoqiang Zheng. TensorFlow: Large-scale machine learning on heterogeneous systems, 2015. URL <http://tensorflow.org/>. Software available from tensorflow.org.
- Omer Abramovich and Amiram Moshaiov. Multi-objective topology and weight evolution of neuro-controllers. In *2016 IEEE congress on evolutionary computation (CEC)*, pages 670–677. IEEE, 2016.
- Peter Auer. Using confidence bounds for exploitation-exploration trade-offs. *Journal of Machine Learning Research*, 3(Nov):397–422, 2002.
- Yoshua Bengio, Nicholas Léonard, and Aaron C. Courville. Estimating or propagating gradients through stochastic neurons for conditional computation. *CoRR*, abs/1308.3432, 2013. URL <http://arxiv.org/abs/1308.3432>.
- Sébastien Bubeck, Nicolo Cesa-Bianchi, et al. Regret analysis of stochastic and nonstochastic multi-armed bandit problems. *Foundations and Trends® in Machine Learning*, 5(1):1–122, 2012.
- Jeffrey Dean, Greg Corrado, Rajat Monga, Kai Chen, Matthieu Devin, Mark Mao, Marc’ aurelio Ranzato, Andrew Senior, Paul Tucker, Ke Yang, et al. Large scale distributed deep networks. In *Advances in neural information processing systems*, pages 1223–1231, 2012.
- Kalyanmoy Deb and Himanshu Jain. NSGA III - An Evolutionary Many-Objective Optimization Algorithm Using Reference-point Based Non-dominated Sorting Approach, Part I. *Ieeexplore.Ieee.Org*, 18(c):1–1, 2013. ISSN 1089-778X. URL http://ieeexplore.ieee.org/lpdocs/epic03/wrapper.htm?arnumber=6600851%5Cnhttp://ieeexplore.ieee.org/xpls/abs_all.jsp?arnumber=6600851.
- Jia Deng, Wei Dong, Richard Socher, Li-Jia Li, Kai Li, and Li Fei-Fei. Imagenet: A large-scale hierarchical image database. In *2009 IEEE conference on computer vision and pattern recognition*, pages 248–255. Ieee, 2009.
- Jacob Devlin, Ming-Wei Chang, Kenton Lee, and Kristina Toutanova. Bert: Pre-training of deep bidirectional transformers for language understanding. *arXiv preprint arXiv:1810.04805*, 2018.
- Zhen Dong, Zhewei Yao, Yaohui Cai, Daiyaan Arfeen, Amir Gholami, Michael W. Mahoney, and Kurt Keutzer. HAWQ-V2: Hessian aware trace-weighted quantization of neural networks. *arXiv*, 12:1–13, 2019. ISSN 23318422.
- Steven K. Esser, Jeffrey L. McKinstry, Deepika Bablani, Rathinakumar Appuswamy, and Dharmendra S. Modha. Learned step size quantization. In *8th International Conference on Learning Representations, ICLR 2020, Addis Ababa, Ethiopia, April 26-30, 2020*. OpenReview.net, 2020. URL <https://openreview.net/forum?id=rkg066VKDS>.
- Hongyang Gao and Shuiwang Ji. Graph u-nets. In *international conference on machine learning*, pages 2083–2092. PMLR, 2019.
- Amir Gholami, Sehoon Kim, Zhen Dong, Zhewei Yao, Michael W. Mahoney, and Kurt Keutzer. A survey of quantization methods for efficient neural network inference. *CoRR*, abs/2103.13630, 2021. URL <https://arxiv.org/abs/2103.13630>.

- Hai Victor Habi, Roy H Jennings, and Arnon Netzer. Hmq: Hardware friendly mixed precision quantization block for cnns. *arXiv preprint arXiv:2007.09952*, 2020.
- Michael Pilegaard Hansen and Andrzej Jaszkievicz. *Evaluating the quality of approximations to the non-dominated set*. Citeseer, 1994.
- Matan Haroush, Itay Hubara, Elad Hoffer, and Daniel Soudry. The knowledge within: Methods for data-free model compression. In *2020 IEEE/CVF Conference on Computer Vision and Pattern Recognition (CVPR)*, pages 8491–8499, 2020. doi: 10.1109/CVPR42600.2020.00852.
- Kaiming He, Xiangyu Zhang, Shaoqing Ren, and Jian Sun. Deep residual learning for image recognition. In *Proceedings of the IEEE conference on computer vision and pattern recognition*, pages 770–778, 2016.
- Sambhav R. Jain, Albert Gural, Michael Wu, and Chris Dick. Trained uniform quantization for accurate and efficient neural network inference on fixed-point hardware. *CoRR*, abs/1903.08066, 2019. URL <http://arxiv.org/abs/1903.08066>.
- Zohar Karnin, Tomer Koren, and Oren Somekh. Almost optimal exploration in multi-armed bandits. In *International Conference on Machine Learning*, pages 1238–1246, 2013.
- Shauharda Khadka, Somdeb Majumdar, Tarek Nassar, Zach Dwiell, Evren Tumer, Santiago Miret, Yinyin Liu, and Kagan Tumer. Collaborative evolutionary reinforcement learning. *arXiv preprint arXiv:1905.00976v2*, 2019.
- Shauharda Khadka, Estelle Aflalo, Mattias Marder, Avrech Ben-David, Santiago Miret, Shie Manor, Tamir Hazan, Hanlin Tang, and Somdeb Majumdar. Optimizing memory placement using evolutionary graph reinforcement learning. *arXiv preprint arXiv:2007.07298*, 2020.
- Thomas N Kipf and Max Welling. Semi-supervised classification with graph convolutional networks. *arXiv preprint arXiv:1609.02907*, 2016.
- Abdullah Konak, David W. Coit, and Alice E. Smith. Multi-objective optimization using genetic algorithms: A tutorial. *Reliability Engineering and System Safety*, 91(9):992–1007, 2006. ISSN 09518320. doi: 10.1016/j.ress.2005.11.018.
- Alexander Kozlov, Ivan Lazarevich, Vasily Shamporov, Nikolay Lyalyushkin, and Yury Gorbachev. Neural Network Compression framework for fast model inference. *arXiv*, 2020. ISSN 23318422.
- Raghuraman Krishnamoorthi. Quantizing deep convolutional networks for efficient inference: A whitepaper. *arXiv preprint arXiv:1806.08342*, 2018.
- Alex Krizhevsky, Vinod Nair, and Geoffrey Hinton. Cifar-10 (canadian institute for advanced research). URL <http://www.cs.toronto.edu/~kriz/cifar.html>.
- Steven Künzel and Silja Meyer-Nieberg. *Coping with opponents: multi-objective evolutionary neural networks for fighting games*, volume 32. 2020. ISBN 0123456789. doi: 10.1007/s00521-020-04794-x.
- Alexandre Lacoste, Alexandra Luccioni, Victor Schmidt, and Thomas Dandres. Quantifying the carbon emissions of machine learning. *arXiv preprint arXiv:1910.09700*, 2019.
- Yuhang Li, Ruihao Gong, Xu Tan, Yang Yang, Peng Hu, Qi Zhang, Fengwei Yu, Wei Wang, and Shi Gu. Brecq: Pushing the limit of post-training quantization by block reconstruction. *arXiv preprint arXiv:2102.05426*, 2021.
- Risto Miikkulainen. Neuroevolution. In C. Sammut, Webb, and G. I., editors, *Encyclopedia of Machine Learning, 2nd Edition*. Springer, Berlin, 2015. URL <http://nn.cs.utexas.edu/?miikkulainen:encyclopedia15-ne>.
- Markus Nagel, Mart Van Baalen, Tijmen Blankevoort, and Max Welling. Data-free quantization through weight equalization and bias correction. In *2019 IEEE/CVF International Conference on Computer Vision (ICCV)*, pages 1325–1334, 2019. doi: 10.1109/ICCV.2019.00141.
- Adam Paszke, Sam Gross, Francisco Massa, Adam Lerer, James Bradbury, Gregory Chanan, Trevor Killeen, Zeming Lin, Natalia Gimelshein, Luca Antiga, Alban Desmaison, Andreas Kopf, Edward Yang, Zachary DeVito, Martin Raison, Alykhan Tejani, Sasank Chilamkurthy, Benoit Steiner, Lu Fang, Junjie Bai, and Soumith Chintala. Pytorch: An imperative style, high-performance deep learning library. In H. Wallach, H. Larochelle, A. Beygelzimer, F. d'Alché-Buc, E. Fox, and R. Garnett, editors, *Advances in Neural Information Processing Systems 32*, pages 8024–8035. Curran Associates, Inc., 2019. URL <http://papers.neurips.cc/paper/>

- 9015-pytorch-an-imperative-style-high-performance-deep-learning-library.pdf.
- Andres Rodriguez, Barukh Ziv, Evarist M Fomenko, Etay Meiri, and Haihao Shen. Lower numerical precision deep learning inference and training. Technical report, January 2018.
- Mark Sandler, Andrew Howard, Menglong Zhu, Andrey Zhmoginov, and Liang-Chieh Chen. Mobilenetv2: Inverted residuals and linear bottlenecks. In *Proceedings of the IEEE conference on computer vision and pattern recognition*, pages 4510–4520, 2018.
- Jacob Schrum and Risto Miikkulainen. Discovering multimodal behavior in ms. pac-man through evolution of modular neural networks. *IEEE Transactions on Computational Intelligence and AI in Games*, 8(1):67–81, March 2016. URL <http://nn.cs.utexas.edu/?schrum:tciaig16>.
- Kenneth O Stanley and Risto Miikkulainen. Evolving neural networks through augmenting topologies. *Evolutionary computation*, 10(2):99–127, 2002.
- K Steven. for Multi-objective Tasks. pages 671–686, 2018. doi: 10.1007/978-3-319-77538-8.
- Felipe Petroski Such, Vashisht Madhavan, Edoardo Conti, Joel Lehman, Kenneth O Stanley, and Jeff Clune. Deep neuroevolution: Genetic algorithms are a competitive alternative for training deep neural networks for reinforcement learning. *arXiv preprint arXiv:1712.06567*, 2017.
- Stefan Uhlich, Lukas Mauch, Fabien Cardinaux, Kazuki Yoshiyama, Javier Alonso Garcia, Stephen Tiedemann, Thomas Kemp, and Akira Nakamura. Mixed precision dnns: All you need is a good parametrization. *arXiv preprint arXiv:1905.11452*, 2019.
- Willem van Willigen, Evert Haasdijk, and Leon Kester. Fast, comfortable or economical: evolving platooning strategies with many objectives. In *16th International IEEE Conference on Intelligent Transportation Systems (ITSC 2013)*, pages 1448–1455. IEEE, 2013.
- Kuan Wang, Zhijian Liu, Yujun Lin, Ji Lin, and Song Han. Haq: Hardware-aware automated quantization with mixed precision. *CVPR*, 2019.
- Bichen Wu, Yanghan Wang, Peizhao Zhang, Yuandong Tian, Peter Vajda, and Kurt Keutzer. Mixed precision quantization of convnets via differentiable neural architecture search. *CoRR*, abs/1812.00090, 2018. URL <http://arxiv.org/abs/1812.00090>.
- Saining Xie, Ross Girshick, Piotr Dollár, Zhuowen Tu, and Kaiming He. Aggregated residual transformations for deep neural networks. In *Proceedings of the IEEE conference on computer vision and pattern recognition*, pages 1492–1500, 2017.
- Zhewei Yao, Zhen Dong, Zhangcheng Zheng, Amir Gholami, Jiali Yu, Eric Tan, Leyuan Wang, Qijing Huang, Yida Wang, Michael W. Mahoney, and Kurt Keutzer. HAWQV3: Dyadic Neural Network Quantization. pages 1–18, 2020. URL <http://arxiv.org/abs/2011.10680>.
- Rex Ying, Ruining He, Kaifeng Chen, Pong Eksombatchai, William L Hamilton, and Jure Leskovec. Graph convolutional neural networks for web-scale recommender systems. In *Proceedings of the 24th ACM SIGKDD International Conference on Knowledge Discovery & Data Mining*, pages 974–983, 2018.

A Computation Details

We consider the computation costs for our method in Section 3 to have two distinct parts: 1. Search; 2. Fine-Tuning. In the case of search, the primary compute bottleneck the evaluation of the simulated quantized network, described in Appendix B, which takes ~ 60 seconds on a hardware unit with 1 GPU and 7 CPU cores. We parallelize the search with 10 parallel search instances to speed the wall-clock time of our experiments and obtain the following approximate compute cost:

Experiment	Evaluation Core Time	Number of Evaluations	Core Time (Total)	Wall Clock (Total)
MobileNetV2	$\sim 60s$	30,000	500 hours	48 hours
ResNet50	$\sim 60s$	30,000	500 hours	48 hours
ResNext101-32x-8d	$\sim 60s$	30,000	500 hours	48 hours

Table 3: NEMO Search Computation Details

For fine-tuning we leverage a multi-GPU setup to improve compute performance. Given that each run is independent, we can leverage linear scaling to parallelize the wall-clock time compute. Here is an approximation of the compute requirements for our experiments:

Experiment	Hardware Details	Core Time (Unit)	Number of Experiments	Core Time (Total)
MobileNetV2	2 GPU, 14 CPU	12 hours	70	840 hours
ResNet50	4 GPU, 28 CPU	12 hours	80	960 hours
ResNext101-32x-8d	4 GPU, 28 CPU	36 hours	30	1080 hours

Table 4: Fine-Tuning Computation Details

The total GPU compute time for our experiment was $\sim 10,000$ GPU hours, which leads to a carbon emissions estimate of $\sim 1,000$ kgCO₂eq using the MachineLearning Impact calculator presented in Lacoste et al. [2019].

A.1 Discussion on Environmental Impact

One potential negative societal impact of the proliferation of additional compute demand for compression techniques is that workload training costs may continue to increase. One particular worrisome scenario would be that large models will be trained once for performance and then re-trained for compression, significantly extending the training resources required. Moreover, even if further efficiency increases in compression or other techniques manage to reduce the cost of training and deployment, potential rebound effects could negate those improvement as greater use could ultimately lead to more compute demand and its resulting emissions. As such, we believe it is important to continue to track and measure the cost of model training and deployment over the lifetime of a given workload. Additionally, we believe it would be useful to also measure the potential savings of model compression during inference to better understand whether compute efficiency increases can offset the cost of actually performing model compression. This would lead to formulating a payback period, meaning that if a workload is deployed for at least X hours, the compute cost of performing the compression before deployment are offset by the savings gained during deployment.

B Simulated Quantization

Given the lack of hardware support for lower integer precisions, a quantized neural network execution graph usually contains quantization and dequantization operation nodes to map tensors back and forth between full-precision to device-supported integer precisions. Many quantization studies, including our own, apply this type of *fake* or *simulated* quantization because this process can be performed on any general-purpose hardware regardless of lower precision support. Simulated quantization effectively maps the integer values given by Equation (1) shown in Section 3.1 back to full-precision values during execution on the hardware, where the fake-quantized tensor of weight \hat{w} and activation

$\hat{\mathbf{a}}$ can be written as:

$$\hat{\mathbf{w}} = Q_w(\mathbf{w}, b_w); \hat{\mathbf{a}} = Q_a(\mathbf{a}, b_a) \text{ where } Q(x; b) = s \cdot q(\mathbf{x}; b)$$

C Implementation Details

C.1 Graph Embedding

Table 5 describes the features included in each node of our graph representation of a given neural network workload. We applied nine features that describe each layer in the workload:

Node Features	Description
o_{pid}	One-hot encoding of layer type
n_{cin}	Input channel size for convolutional layer; 0 otherwise
c_{cout}	Output channel size for convolutional layer; 0 otherwise
i_{dw}	True if depthwise-seeperable convolution layer; false otherwise
$n_{feature}$	input feature map size for convolutional layer, number of input features for fully-connected layer; 0 otherwise
n_{kernel}	Kernel patch size for convolutional layer; 0 otherwise
n_{param}	Number of learnable parameters in the layer
n_{stride}	Step size of convolution stride; 0 for non-convolutional layer
i_{wq}	True for layers with parameters that require weight quantization, False otherwise

Table 5: Graph Node Features

Table 6 shows the hyperparameters for the GNN species, Graph-Conv and Graph-UNet, in our experiments.

Hyperparameter	Value
Graph-UNet Depth	3
Graph-UNet Attention Heads	4
Graph-UNet Hidden Sizes	10, 8
Graph-Conv-Net Attention Heads	4
Graph-Conv-Net Hidden Sizes	10, 8

Table 6: NEMO Species Hyperparameters

Table 7 shows the hyperparameters for the NEMO search algorithms specifically. The search algorithm hyperparameters are separate and additional to the hyperparameters within each species in Table 6

Hyperparameter	Value
Number of Objectives	3
Uniform Reference Points	25
UCB Coefficient	0.9
Crossover Probability	1.0
Mutation Operation Probability	1.0
Neuroevolution Mutation Fraction	0.05
Neuroevolution Mutation Strength	0.1
Stateless Mutation Strength	0.05

Table 7: NEMO Search Hyperparameters

D Pareto Optimal Frontiers

D.1 MobileNet-V2

We show heatmap plots for the full NEMO search results and 3D Pareto frontier for MobileNet-V2. The initial search yields a good amount of suboptimal mappings, which are filtered out when creating the Pareto frontier of 384 unique solutions. We then downselect a region spanning $0.07 \leq \text{model-ratio} \leq 0.20$, $0.05 \leq \text{bit-ops} \leq 0.20$ in the Pareto optimal set for further fine-tuning as shown by the red rectangular region in Figure D.1 that includes a critical region of severe accuracy drop-offs. Our final, fine-tuned NEMO Pareto front shown in Figure D.1 contains 112 unique solutions.

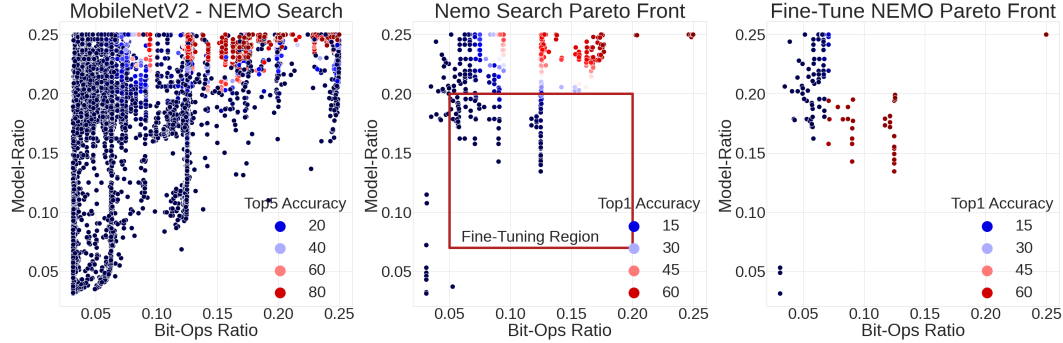


Figure D.1: Heatmap Scatterplot of MobileNetV2 results with full NEMO search results (left), the Pareto optimal set of the NEMO search with selected fine-tuning region (middle), and final Pareto optimal set after fine-tuning

Additionally, we present the 2D projections of the full three dimensional Pareto front for model-ratio and bit-operations. In Section 4 we discuss and compare the point in relevant neighborhoods. The model-ratio curve shows steep decrease in accuracy in a crowded field of solutions, while the bit-operations curve shows a gap in solutions between 0.6 and 0.12.

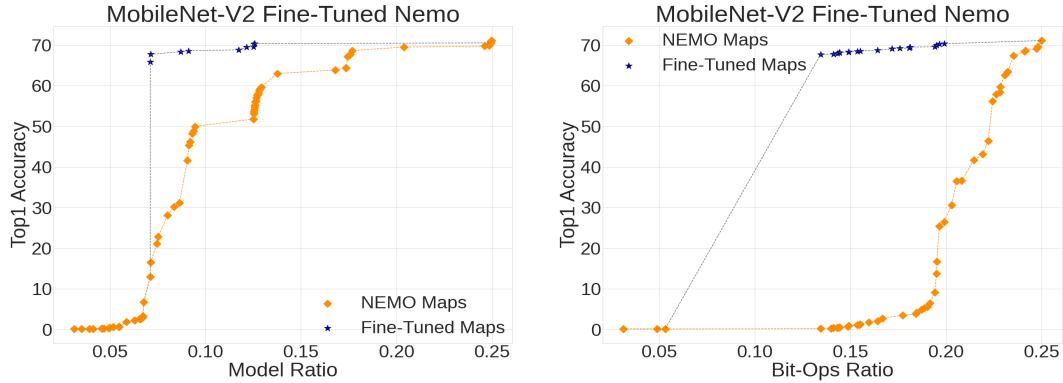


Figure D.2: MobileNetV2: Two-Dimensional Projections of Pareto Fronts for Top1-Accuracy vs Model-Ratio (left) and Top1-Accuracy vs Bit-Ops (right)

D.2 ResNet50

We show heatmap plots for the full NEMO search results and 3D Pareto frontier for ResNet50. We determine 266 Pareto optimal configurations for which we select a fine-tuning region spanning $0.08 \leq \text{model-ratio} \leq 0.20$, $0.08 \leq \text{bit-ops} \leq 0.13$ as shown in red rectangular region in Figure D.3. The final fine-tuned NEMO Pareto set includes 73 unique optimal configurations.

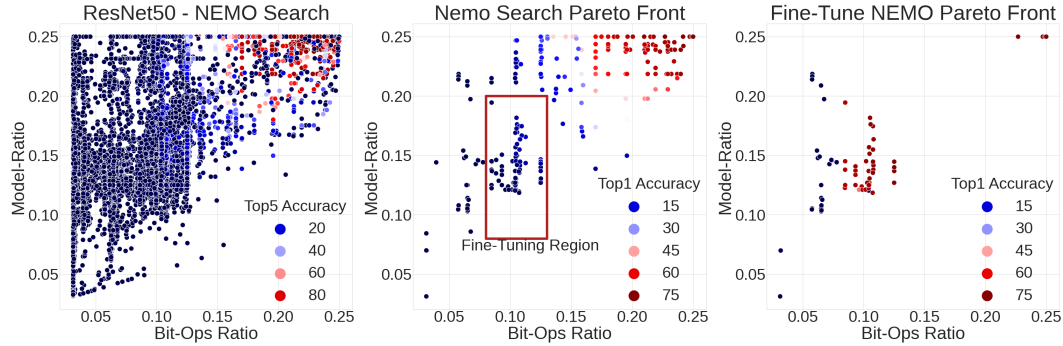


Figure D.3: Heatmap Scatterplot of ResNet50 Results with full NEMO search results (left), the Pareto optimal set of the NEMO search with highlighted fine-tuning region (middle), and final Pareto optimal set after fine-tuning

Additionally, we present the 2D projections of the full three dimensional Pareto front for model-ratio and bit-operations. In Section 4 we discuss and compare the point in relevant neighborhoods. Both model-ratio curve and the bit-operations frontiers show steep decreases in accuracy in a crowded field of solutions.

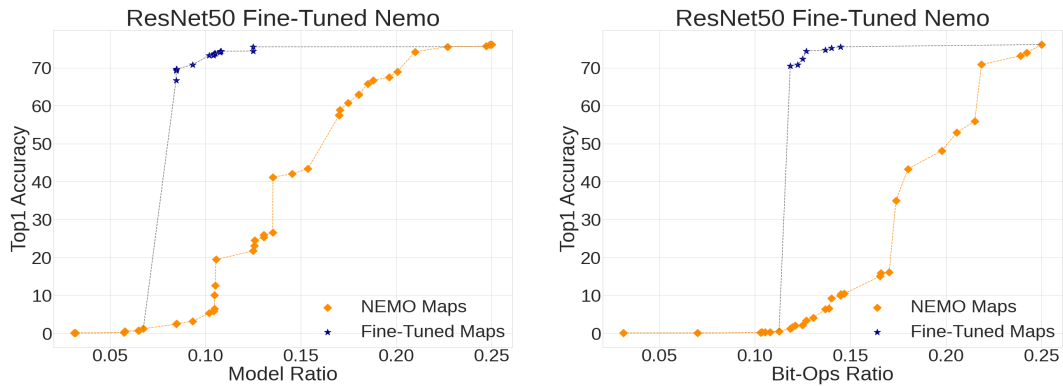


Figure D.4: ResNet50: Two-Dimensional Projections of Pareto Fronts for Top1-Accuracy vs Model-Ratio (left) and Top1-Accuracy vs Bit-Ops (right)